

# Transmission spectra of two-dimensional quantum structures

Kia Manouchehri and J.B. Wang\*

*School of Physics, The University of Western Australia*

(Dated: November 10, 2018)

## Abstract

To study the ballistic transport of charge carriers in nano-structured quantum devices, a highly efficient numerical technique is developed, which provides continuous transmission spectra for arbitrarily complex potential geometries in two dimensions. We apply the proposed method to single and double barrier structures and compare the results with those obtained using standard techniques for computing transmission coefficients. Excellent numerical agreement as well as considerable computational saving is demonstrated.

Keywords: nano-structures, electron transport, transmission spectra, quantum dynamics, time domain

arXiv:quant-ph/0408114v3 5 Sep 2006

---

\*Electronic address: wang@physics.uwa.edu.au

## I. INTRODUCTION

A wide range of potential applications for nano-scale electronics in the quantum regime, together with a rapid increase in computing power, have generated much interest in the numerical analysis of nano-structured devices as a viable means for studying their properties [1, 2, 3, 4]. Examples of such applications based on the transport properties of ballistic charge-carriers include quantum wires [5, 6, 7, 8, 9], quantum resistors [10], resonant tunnelling diodes and band filters [11, 12], quantum transistors and stub tuners [13, 14, 15], quantum switches [16], quantum sensors [17, 18, 19], as well as qubits and quantum logic gates [20, 21].

Much insight into the behavior of such devices can be gained by studying the energy dependance of transmission through various nano-structures for propagating charge carriers. The transmission coefficient of a propagating wave function can be determined by the application of time-independent (static) or time-dependent (dynamic) techniques [22]. The time-independent approach involves solving the time-independent Schrödinger equation, commonly carried out using one of three methods: (1) Mode matching method which is based on splitting the nano-structures into different regions with known analytical solution. The total wave function is then derived by matching the solutions at the boundary between regions. This method has been widely used to study quantum devices with simple geometries [23, 24, 25, 26]. In principle, any arbitrary structure can be divided into many segments, each of which is approximated as a rectangular potential well with a finite width. For complex geometries however, this can result in a very large matrix to be inverted and the computation can become unstable. (2) Finite element method [27] where using an irregular numerical mesh, the potential and the wave function are discretized by choosing a suitable set of basis functions to approximate each grid point. However, due to the approximate nature of the elemental solutions, large grids are still required for accurately representing the wave function particularly when dealing with excited or continuous energy states. This often results in an excessive computational cost as well as the introduction of high frequency noise, which can considerably distort the phase of the wave function. (3) Green's function method [28, 29] where the Schrödinger's equation is expressed and solved using the common Green's function techniques. Although in principle capable of providing solutions to arbitrarily complex problems independently of the potential boundary structures, the Green's

function method is most efficient when used in conjunction with simplifying assumptions such as the decoupling of the  $x$  and  $y$  variables in the two-dimensional Schrödinger equation or by not requiring information about a global wave function. In particular, the later case leads to an efficient algorithm for calculating the transmission coefficients known as the recursive Green's function method [30], where it is necessary to compute the Green's function only for some sections of the structure. The calculation of the wave function for a general two-dimensional case however relies on computing the generalized Green's function for the entire region, which is computationally expensive.

As well as their limited utility in constructing global wave functions for complex nanostructure geometries efficiently, the time-independent methods are also unable to provide information on the transient behavior of the system under study. This can be addressed by solving the time-dependent Schrödinger equation where transmission coefficients are obtained by numerically propagating an initial wave function through a given potential geometry and then summing over the transmitted parts. Methods for solving the time-dependent Schrödinger equation include: (1) The finite difference method [31, 32], which uses an  $n$ th order finite difference approximation to expand the time-evolution operator. This method however suffers from a low convergence rate as well as excessive truncation errors over modestly long propagation times. (2) Split operator method [33], where the time-evolution operator is approximated as the product of three diagonal operators which can be readily solved. This scheme however neglects the commutator between these operators and thus introduces error in both energy and phase of the wave function. (3) The time-dependent Green's functions method [34], which employs the standard Green's function techniques. Due to its reliance on summations over a large number of energy-eigenstates however, this method too becomes computationally prohibitive when dealing with complex potentials. (4) Chebyshev-Fourier propagation scheme, which is based on expressing the evolution operator using the Chebyshev approximation [35]. This method proves to be numerically robust as well as efficient for propagations over arbitrary potentials.

Nonetheless, when approached naively, calculating the transmission coefficients for a wide range of energies using the Chebyshev-Fourier scheme could still prove computationally expensive, amounting to repeated propagations of an initial wave function with various mean energies in the given range. A novel method for computing the transmission coefficients was developed by Yin and Wang [36], which arrives at the entire transmission spectrum for a

given range of energies after only one propagation of an initial wave function with a broad energy distribution. Although this method is shown to be highly efficient while maintaining the capacity to deal with arbitrary potentials in one dimension, its use in two dimensions is limited to geometries with infinite boundary conditions in the second dimension and decoupled  $x$  and  $y$  variables [36, 37].

In this paper we extend the work of Yin and Wang [36], making it possible to treat arbitrarily complex potentials in two dimensions, without imposing any limitations on the dimensional parameters of the system, such as decoupling in the  $x$  and  $y$  directions. We apply this scheme to single and double hyperbolic barrier structures and demonstrate excellent numerical accuracy while maintaining a high degree of computational efficiency, compared to standard techniques for obtaining individual transmission coefficients.

## II. THEORY

We begin by considering the two-dimensional Schrödinger equation

$$i\hbar\frac{\partial}{\partial t}\psi(x, y, t) = \hat{H}\psi(x, y, t), \quad (1)$$

where the Hamiltonian  $\hat{H}$  is given by

$$\hat{H} = -\frac{\hbar^2}{2m^*}\nabla^2 + V(x, y, t) \quad (2)$$

with  $m^*$  being the effective mass of the propagating charge carrier within the semiconducting lattice. If the potential function is time-independent i.e  $V(x, y, t) \equiv V(x, y)$ , then a formal solution to this equation is

$$\psi(x, y, t) = \exp\left(-\frac{i}{\hbar}\hat{H}t\right)\psi(x, y, 0) \quad (3)$$

where  $t$  is the propagation time, and  $\exp\left(-\frac{i}{\hbar}\hat{H}t\right)$  is the time evolution propagator, commonly denoted by  $\hat{U}$ . The Chebyshev-Fourier scheme as detailed in [35, 38] approximates  $\hat{U}$  by a Chebyshev polynomial expansion

$$\psi(x, y, t) = \exp[-i(\mathcal{E}_{max} + \mathcal{E}_{min})t] \sum_{n=0}^{\mathcal{N}} a_n(\alpha)\phi_n(-\tilde{\mathcal{H}})\psi(x, y, 0) \quad (4)$$

where  $\mathcal{E}_{min}$  and  $\mathcal{E}_{max}$  are the upper and lower bounds on the energies sampled by the wave packet,  $a_n(\alpha) = 2J_n(\alpha)$  except for  $a_0(\alpha) = J_0(\alpha)$ ,  $J_n(\alpha)$  are the Bessel functions of the first

kind,  $\phi_n$  are the Chebyshev polynomials, and  $\mathcal{N}$  is the number of terms in the Chebyshev expansion. To ensure convergence, the Hamiltonian needs to be normalized as

$$\tilde{\mathcal{H}} = \frac{1}{\mathcal{E}_{max} - \mathcal{E}_{min}} [2\hat{H} - \mathcal{E}_{max} - \mathcal{E}_{min}]. \quad (5)$$

The action of the Laplacian operator  $\nabla$  on the wave functions is carried out using a Fourier transformation technique [38]. It is important to note that the rapid convergence and the high numerical accuracy of this propagation scheme are well established in the literature [4, 35, 38, 39, 40], where it has been used in the study of various quantum nano-structures.

In the simulations we start with a localized wave packet as the initial wave function  $\psi_i = \psi(x, y, t = 0)$  and then use the Chebyshev-Fourier scheme as a means to propagate this wave packet in time  $t$ . The final wave function  $\psi_f = \psi(x, y, t = \tau)$  is partly transmitted and partly reflected due to the potential barrier  $V(x, y)$  (Fig. 1). To evaluate the transmission coefficient  $T(\bar{\mathcal{E}})$  for any given potential barrier, one can setup  $\psi_i$  with an incident mean energy  $\bar{\mathcal{E}}$  and a very small energy uncertainty, propagate  $\psi_i$  in time until it is completely scattered by the barrier, and then collect the transmitted parts of  $\psi_f$ . In this way, obtaining a transmission spectrum entails multiple propagations for different incident energies as depicted in Fig. 3. Given the computational cost associated with any time-dependant propagation scheme however, the use of this *direct method* for obtaining a continuous transmission spectrum is clearly inefficient.

In Yiu and Wang's approach [36], a wave packet with a small spatial uncertainty (corresponding to a large momentum spread) is used to obtain the entire transmission curve after only one propagation. In other words, one can compute the transmission coefficients by simply transforming the transmitted wave packet to momentum space and dividing by the original momentum space wave function. Noting that in one dimension, the transmitted and reflected wave packets can be expressed as momentum space components of  $\psi_f$  with positive momentum ( $p > 0$ ) and negative momentum ( $p < 0$ ) respectively, one can then write

$$T(p) = \frac{|\psi_f(p > 0)|^2}{|\psi_i(p)|^2} \quad \text{and} \quad R(p) = \frac{|\psi_f(p < 0)|^2}{|\psi_i(p)|^2}, \quad (6)$$

where  $T(p)$  and  $R(p)$  are the transmission and reflection coefficients at momentum  $p$ . This scheme however, is strictly limited to scattering in one dimension. In order to show this we present a more generalized approach to the problem, which enables us to extend the current scheme to two dimensions.

First we note that in principal  $\psi(x, y, t)$  may be expressed as a linear superposition of energy eigenfunctions  $\phi_E(x, y)$ . We can therefore rewrite Eq. (3) as

$$\psi(x, y, t) = e^{-i\hat{H}t/\hbar} \sum_E^{\dagger} c_i(E) \phi_E(x, y) \quad (7)$$

$$= \sum_E^{\dagger} e^{-iEt/\hbar} c_i(E) \phi_E(x, y) \quad (8)$$

$$= \sum_E^{\dagger} c_f(E) \phi_E(x, y) , \quad (9)$$

where  $c_i(E)$  and  $c_f(E)$  denote the initial and final complex coefficients associated with each energy eigenfunction. We note that  $c_i(E)$  and  $c_f(E)$  only differ by a phase factor. Expressing  $c_f(E)$  as  $\langle E|\psi_f\rangle$  we can expand  $c_f(E)$  using the position basis set

$$c_f(E) = \iint \langle E|x, y\rangle \langle x, y|\psi_i\rangle dx dy \quad (10)$$

$$|c_f(E)|^2 = \iint \langle E|x, y\rangle \langle x, y|\psi_f\rangle \langle \psi_f|E\rangle dx dy \quad (11)$$

In the position space however the final wave function assumes two components: the transmitted part lying in an area  $T$ , and the reflected part lying in an area  $R$ . Noting that these two areas do not overlap we can write

$$|c_f(E)|^2 = \iint_T \langle E|x, y\rangle \langle x, y|\psi_f\rangle \langle \psi_f|E\rangle dx dy \quad (12)$$

$$+ \iint_R \langle E|x, y\rangle \langle x, y|\psi_f\rangle \langle \psi_f|E\rangle dx dy \quad (13)$$

$$= |c_T(E)|^2 + |c_R(E)|^2 \quad (14)$$

where  $c_T(E)$  and  $c_R(E)$  are the transmission and reflection coefficients of each energy eigenfunction. We therefore conclude that

$$|c_i(E)|^2 = |c_f(E)|^2 = |c_T(E)|^2 + |c_R(E)|^2 . \quad (15)$$

In other words the amplitude of each energy eigenfunction will independently conserve throughout the propagation and must therefore have its own transmitted and reflected parts.

In order to evaluate  $|c_i(E)|^2$ ,  $|c_T(E)|^2$  and  $|c_R(E)|^2$ , we consider the case where the initial and the scattered wave functions are both sufficiently distant from the potential barrier, such that the interaction between the wave function and the potential barrier is negligible,

i.e.  $\langle \psi | \hat{V} | \psi \rangle \rightarrow 0$ . As a result we can ignore the contribution of the potential term  $V(x, y)$  in the Hamiltonian since  $\hat{H} \rightarrow \hat{p}^2/2m^*$ , meaning that energy is directly proportional to the square of the momentum operator.

Now representing the initial wave functions in the momentum space, denoted by  $\psi_i(p_x, p_y) = \frac{1}{2\pi\hbar} \int \int \exp(\frac{-i}{\hbar}(p_x x + p_y y)) \psi_i(x, y) dx dy$ , and noting that the total momentum  $p^2 = p_x^2 + p_y^2$ , we have

$$|c_i(E)|^2 = \sum_{p_x} \sum_{p_y} |\psi_i(p_x, p_y)|^2, \text{ for } p_x^2 + p_y^2 = 2m^*E. \quad (16)$$

In this way computing  $|c_i(E)|^2$  amounts to simply summing over those momentum components which lie on a circle with radius  $\sqrt{2m^*E}$  as depicted in Fig. 2. Furthermore, by defining the motion of the initial wave packet to be in the positive  $x$  direction (see Fig. 1), transmission and reflection can also be conveniently characterized using the momentum space representation of the final wave function  $\psi_f(p_x, p_y)$ . Referring to the momentum circle described above,  $|c_T(E)|^2$  and  $|c_R(E)|^2$  correspond to semicircles with  $p_x > 0$  and  $p_x < 0$  respectively. i.e.

$$|c_T(E)|^2 = \sum_{p_x > 0} \sum_{p_y} |\psi_f(p_x, p_y)|^2, \text{ for } p_x^2 + p_y^2 = 2m^*E, \quad (17)$$

$$|c_R(E)|^2 = \sum_{p_x < 0} \sum_{p_y} |\psi_f(p_x, p_y)|^2, \text{ for } p_x^2 + p_y^2 = 2m^*E. \quad (18)$$

In this way, the transmission coefficient  $T(E)$  can be written as

$$T(E) = \frac{|c_T(E)|^2}{|c_i(E)|^2}. \quad (19)$$

Therefore, in principle, all the transmission coefficients can be calculated after propagating only a single initial wave packet  $\psi_i$  for any choice of  $\bar{\mathcal{E}}$ . In this work we have used an initial wave packet which has a small momentum spread in the  $y$  direction, but a broad momentum distribution in the  $x$  direction, as depicted in Fig. 4. The scattering of this customized wave packet, which we refer to as the *broad-energy wave packet*, provides us with an efficient means for computing the continuous transmission spectrum over a wide range of incident energies for an arbitrary potential barrier in two dimensions. We term this scheme the *momentum space method*.

### III. RESULTS

In this section we demonstrate the use of the momentum space technique to obtain a series of continuous transmission spectra for the scattering of ballistic electrons by the single and double barrier potentials (Fig. 5), positioned at various angles  $\alpha$  with respect to the incident electron (Fig. 1). We then compare the results with transmission coefficients obtained using the direct method (using multiple wave packets with small momentum uncertainty).

The barriers are constructed using hyperbolic functions in the  $x$  direction:  $V(x) = V_0/\cosh^2(\frac{x}{a})$  for the single barrier and  $V(x) = V_0/\cosh^2(\frac{x-d}{a}) + V_0/\cosh^2(\frac{x+d}{a})$  for the double barrier where the barrier height  $V_0 = 13.6$  eV, width parameter  $a = 0.21$  nm (giving a half width of 0.19 nm), and the barrier separation  $2d = 1.58$  nm. Simulations are carried out using three orientation angles  $\alpha = 90^\circ, 62^\circ$ , and  $52^\circ$ .

The incident ballistic electrons are modelled using a Gaussian wave packet

$$\psi(x, y, 0) = \exp\left(-\frac{(x-L)^2}{2\sigma_x^2} - \frac{y^2}{2\sigma_y^2}\right) + i(x\bar{p}_x + y\bar{p}_y)/\hbar, \quad (20)$$

where  $\sigma_x = \hbar/\sqrt{2}\Delta p_x$  and  $\sigma_y = \hbar/\sqrt{2}\Delta p_y$  are the wave packet's standard deviation in the  $x$  and  $y$  dimensions,  $\Delta p_x$  and  $\Delta p_y$  are momentum uncertainty components,  $\bar{p}_x = \sqrt{2m^*\bar{\mathcal{E}}}$  and  $\bar{p}_y = 0$  are the mean momentum components of the wave packet with mean energy  $\bar{\mathcal{E}}$ . In the simulations we consider electron wave packets with effective mass  $m^* = 0.06m_e$  and  $\bar{\mathcal{E}}$  in the range of  $[0.1, 3.5]V_0$ . The narrow-energy wave packets (used in the direct method) have a spacial distribution given by  $\sigma_x = \sigma_y = 7.5$  nm corresponding to  $\Delta E$  in the range of  $[0.02, 0.1]V_0$ , and  $L = 45.0$  nm. The broad-energy wave packets (used in the momentum space method) are characterized by  $\sigma_x = 0.75$  nm and  $\sigma_y = 7.5$  nm, mean energy  $\bar{\mathcal{E}} = 1V_0$ , and  $L = 26.5$  nm. Wave packets are propagated for a time  $t = mD/p_x$  where  $D \approx 3L$  is the propagation distance. The choice of parameters  $L$  and  $D$  ensures that both the initial and final wave functions are sufficiently away from the potential barriers (i.e.  $(\langle \psi | \hat{V} | \psi \rangle / \langle \psi | \hat{H} | \psi \rangle < 10^{-4})$ ). Fig. 6 and 7 illustrate the position space evolution of the broad-energy wave packet for the double barrier potentials with  $\alpha = 90^\circ$  and  $52^\circ$ .

In order to examine the accuracy of the proposed momentum space method, we show firstly that the transmission curves are independent of the choice of  $\bar{\mathcal{E}}$  for the broad-energy wave packets. Fig. 8 presents a transmission curve for the double barrier potential with  $\alpha = 52^\circ$ , constructed by overlapping multiple segments from transmission curves obtained

using initial wave packet with  $\bar{\mathcal{E}}/V_0 = 0.2, 0.6, 1.0, 1.4, 1.8, 2.2, 2.6,$  and  $3.0$  respectively. An excellent match between these segments producing a uniform transmission spectrum is demonstrated.

Secondly, we compare the continuous transmission curves obtained using the momentum space method, against the discrete transmission coefficients obtained using the direct method. Fig. 9 and 10 depict the results for the single and double barrier potentials respectively, with three orientation angles  $\alpha = 52^\circ, 62^\circ$  and  $90^\circ$ . A close match between each transmission curve and its corresponding transmission coefficients (points on each curve) demonstrates an excellent agreement between the two methods.

In order to examine the computational efficiency of the momentum space method, we first note that the accuracy and convergence of the Chebyshev-Fourier propagation scheme primarily depends on the choice of  $\mathcal{E}_{max}$  in Eq. (5), which determines the dimensions of the numerical grid due to Nyquist's sampling theorem. This accuracy improves asymptotically with higher values of  $\mathcal{E}_{max}$  while making computation more costly. In the simulations  $\mathcal{E}_{max}$  is estimated based on the maximum potential energy of the system  $V_0$ , the mean momentum of the initial wave packet, and its maximum momentum range. We then define an accuracy factor  $\beta$  to be the ratio between the actual value of  $\mathcal{E}_{max}$  used in the simulation and the initial estimation. All results from the momentum space method were obtained using  $\beta = 1.0$ , which was found to provide good accuracy while maintaining a reasonable computational speed. The direct method however, at times, required a higher  $\beta$  value for convergence. In the case of the double barrier with  $\alpha = 90^\circ$  for instance, increasing  $\beta$  from  $1.0$  to  $1.2$ , produces no discernable improvements in the resulting transmission curve using the momentum space method (Fig. 11). Using the direct method however, setting  $\beta = 1.0$  leads to significant discrepancies between the transmission points and the transmission curve (Fig. 12). Conversely, setting  $\beta = 2.0$  results in an excellent agreement (Fig. 13), but severely increases the cpu time requirement.

The efficiency of the momentum space scheme becomes particularly apparent when considering the existence of narrow transmission peaks in the spectrum (such as the one at  $\bar{\mathcal{E}} = 0.4V_0$  for the double barrier potential with  $\alpha = 52^\circ$ ). In the above simulations, obtaining a continuous transmission curve using the momentum space method was 5 times faster than the application of the direct method, when requiring only 20 points to represent the same curve. In the absence of prior information about the topography of the transmission

spectrum however, using the direct method necessitates probing the spectrum with a much higher resolution, in order to detect possible narrow transmission peaks. As such, applying the direct method can become prohibitively inefficient, rendering the use of momentum space scheme vastly advantageous.

#### IV. CONCLUSION

We presented an efficient scheme for computing the continuous transmission spectrum of charge carriers scattered by an arbitrary potential geometry in two dimensions. We applied this scheme to single and double barrier potentials at various angles of incidence, and demonstrated excellent precision as well as substantial computational saving as compared to a standard method commonly used for calculating transmission coefficients.

- 
- [1] F. Sols, M. Macucci, U. Ravaioli, and K. Hess, *Appl. Phys. Lett.* **54**, 350 (1989).
  - [2] C. S. Lent and D. J. Kirkner, *J. Appl. Phys.* **67**, 6353 (1990).
  - [3] C. S. Kim, A. M. Satanin, Y. S. Joe, and R. M. Cosby, *Phys. Rev. B* **60**, 10962 (1999).
  - [4] S. Midgley and J. B. Wang, *Phys. Rev. B* **64**, 153304 (2001).
  - [5] T. Sugaya, J. P. Bird, M. Ogura, Y. Sugiyama, D. K. Ferry, and K. Y. Jang, *App. Phys. Lett.* **80**, 434 (2002).
  - [6] B. Kane, G. Facer, A. Dzurak, N. Lumpkin, R. Clark, L. PfeiKer, and K. West, *Appl. Phys. Lett.* **72**, 3506 (1998).
  - [7] C. Dekker, *Physics Today* **52**, 22 (1999).
  - [8] A. Yacoby, H. L. Stormer, N. S. Wingreen, L. N. Pfeiffer, K. W. Baldwin, and K. W. West, *Phys. Rev. Lett.* **77**, 4612 (1996).
  - [9] Y. Hayamizu, M. Yoshita, S. Watanabe, H. A. L. PfeiKer, and K. West, *App. Phys. Lett.* **81**, 4937 (2002).
  - [10] S. Frank, P. Poncharal, Z. L. Wang, and W. A. Heer, *Science* **280**, 1744 (1998).
  - [11] I. Kamiya, I. Tanaka, K. Tanaka, F. Yamada, Y. Shinozuka, and H. Sakaki, *Physica E* **13**, 131 (2002).
  - [12] A. K. Geim, P. C. Main, N. LaScala, L. Eaves, T. J. Foster, P. H. Beton, J. W. Sakai, F. W.

- Sheard, M. Henini, G. Hill, et al., Phys. Rev. Lett. **72**, 2061 (1994).
- [13] J. Appenzeller, C. Schroer, T. Schapers, A. Hart, A. Forster, B. Lengeler, and H. Luth, Phys. Rev. B **53**, 9959 (1996).
- [14] J. Appenzeller and C. Schroer, J. Appl. Phys. **87**, 3165 (2000).
- [15] P. Debray, O. E. Raichev, M. Rahman, R. Akis, and W. C. Mitchel, Appl. Phys. Lett. **74**, 768 (1999).
- [16] A. S. Melnikov and V. M. Vinokur, Nature **415**, 60 (2002).
- [17] K. Schwab, E. A. Henriksen, J. M. Worlock, and M. L. Roukes, Nature **404**, 974 (2000).
- [18] L. Kouwenhoven, Nature **403**, 374 (2000).
- [19] S. Komiyama, O. Astafiev, T. K. V. Antonov, and H. Hirai, Nature **403**, 405 (2000).
- [20] E. Paspalakis, Z. Kis, E. Voutsinas, and A. F. Terzis, Phys. Rev. B **69**, 155316 (2004).
- [21] J. H. Jefferson, M. Fearn, D. L. J. Tipton, and T. P. Spiller, Phys. Rev. A **66**, 042328 (2002).
- [22] J. b. Wang, *The handbook of 'Quantum waveguide theory' in theoretical and computational nano science* (to be published by the American Scientific Publisher, 2005).
- [23] L. Burgnies, O. Vanbesien, and D. Lippens, J. Phys. D: Appl. Phys. **32**, 706 (1999).
- [24] A. Weisshaar, J. Lary, S. M. Goodnick, and V. K. Tripathi, J. Appl. Phys. **70**, 355 (1991).
- [25] G. Jin, Z. Wang, A. Hu, and S. Jiang, J. Appl. Phys. **85**, 1597 (1999).
- [26] C. S. Kim, A. M. Satanin, Y. S. Joe, and R. M. Cosby, Phys. Rev. B **60**, 10962 (1999).
- [27] C. S. Lent and D. J. Kirkner, J. Appl. Phys. **67**, 6353 (1990).
- [28] J. J. Koonen, H. Buhmann, and L. W. Molenkamp, Phys. Rev. Lett. **84**, 2473 (2000).
- [29] E. G. Novik, H. Buhmann, and L. W. Molenkamp, Phys. Rev. B **67**, 245302 (2003).
- [30] F. Sols, M. Macucci, U. Ravaioli, and K. Hess, J. Appl. Phys. **66**, 3892 (1989).
- [31] E. A. McCullough and R. E. Wyatt, J. Chem. Phys. **54**, 3578 (1971).
- [32] A. Asker and A. S. Cakmak, J. Chem. Phys. **68**, 2794 (1978).
- [33] M. D. Feit, J. A. Fleck, and A. Steiger, J. Comp. Phys. **47**, 412 (1982).
- [34] L. Yi and J. S. Wang, Phys. Rev. B **63**, 073304 (2001).
- [35] H. Tal-Ezer and R. Kosloff, J. Chem. Phys. **81**, 3967 (1984).
- [36] C. Yiu and J. Wang, J. Appl. Phys. **80**, 4208 (1996).
- [37] C. Yiu and J. Wang, International Journal of Modern Physics B **13**, 895 (1999).
- [38] J. Wang and S. Midgley, Phys. Rev. B **60**, 13668 (1999).
- [39] P. Falloon and J. Wang, Computer Physics Communications **134**, 167182 (2001).

[40] J. B. Wang and S. Midgley, *Physica B* **284-288**, 1962 (2000).

## V. FIGURES

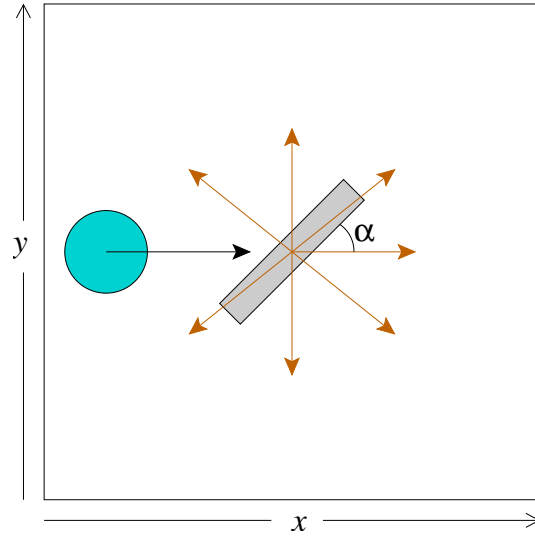


FIG. 1: Position space: the incident particle approaches the scattering potential barrier from the left in the  $x$  direction. The angle  $\alpha$  describes the orientation of the barrier with respect to the incident particle.

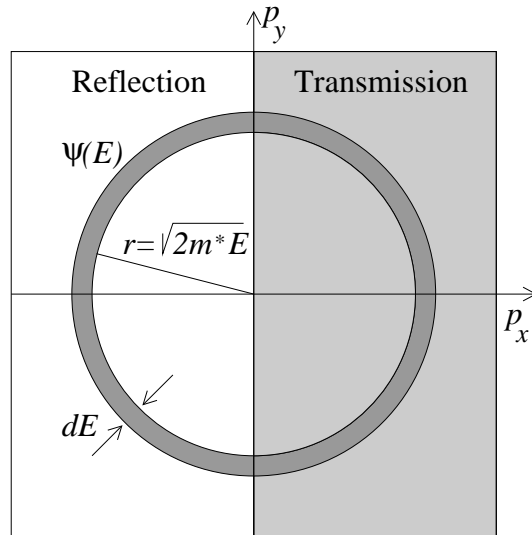


FIG. 2: Momentum space: transmission and reflection are defined as wave components with  $p_x > 0$  and  $p_x < 0$  respectively. Components  $\psi(E)$  correspond to rings of radius  $r = \sqrt{2m^*E}$ .

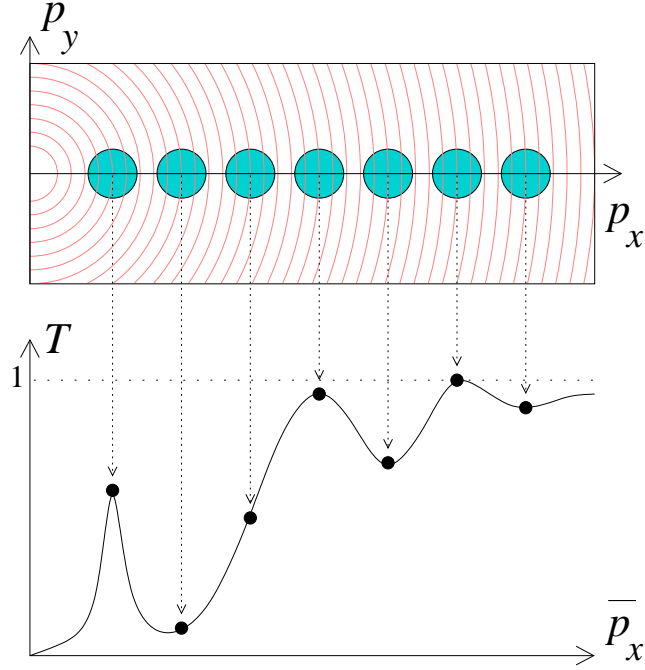


FIG. 3: In the momentum space incident charge carriers are modelled using initial wave packets with a narrow momentum spread, positioned at  $\bar{p}_x = \sqrt{2m^*\bar{\mathcal{E}}}$  and  $\bar{p}_y = 0$ , where  $\bar{\mathcal{E}}$  is the mean energy of the wave packet. A complete transmission curve can be constructed by computing the transmission coefficient of every wave packet with  $\bar{\mathcal{E}}$  in the given range.

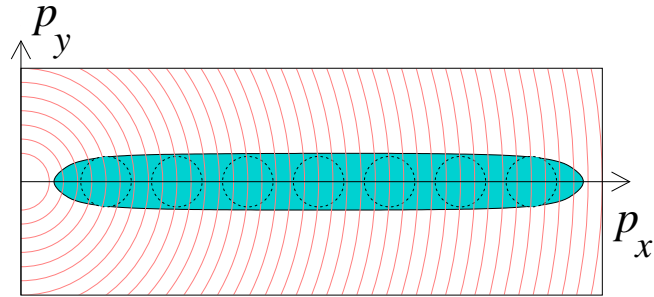


FIG. 4: A broad-energy wave packet has a large momentum spread in the  $x$  direction, corresponding to the energy range of the transmission spectrum. In the  $y$  direction however, it has the same spread as the single charge carrier wave packets.

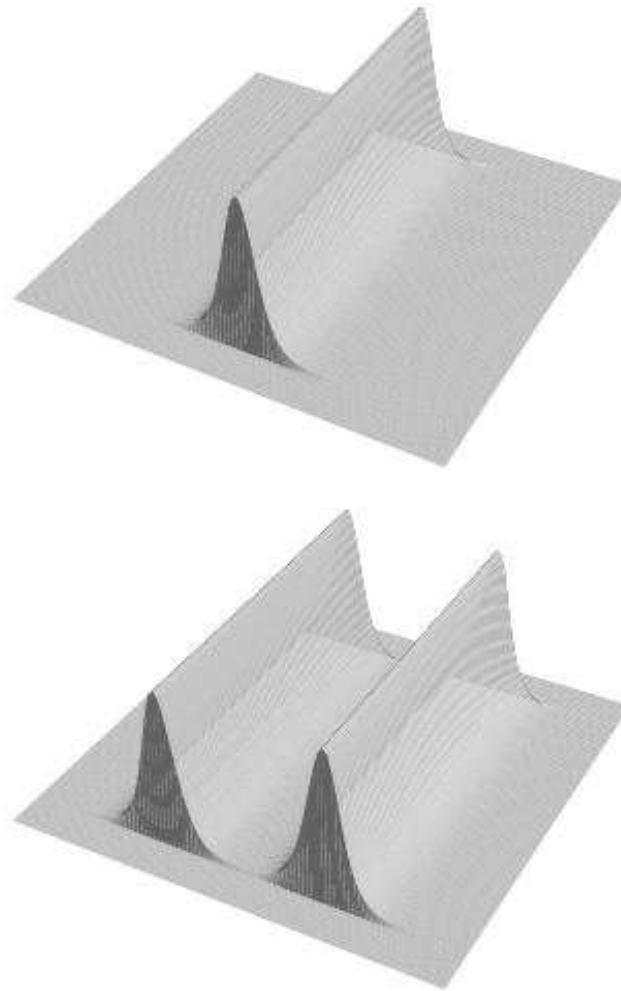


FIG. 5: Single and double barrier potentials.

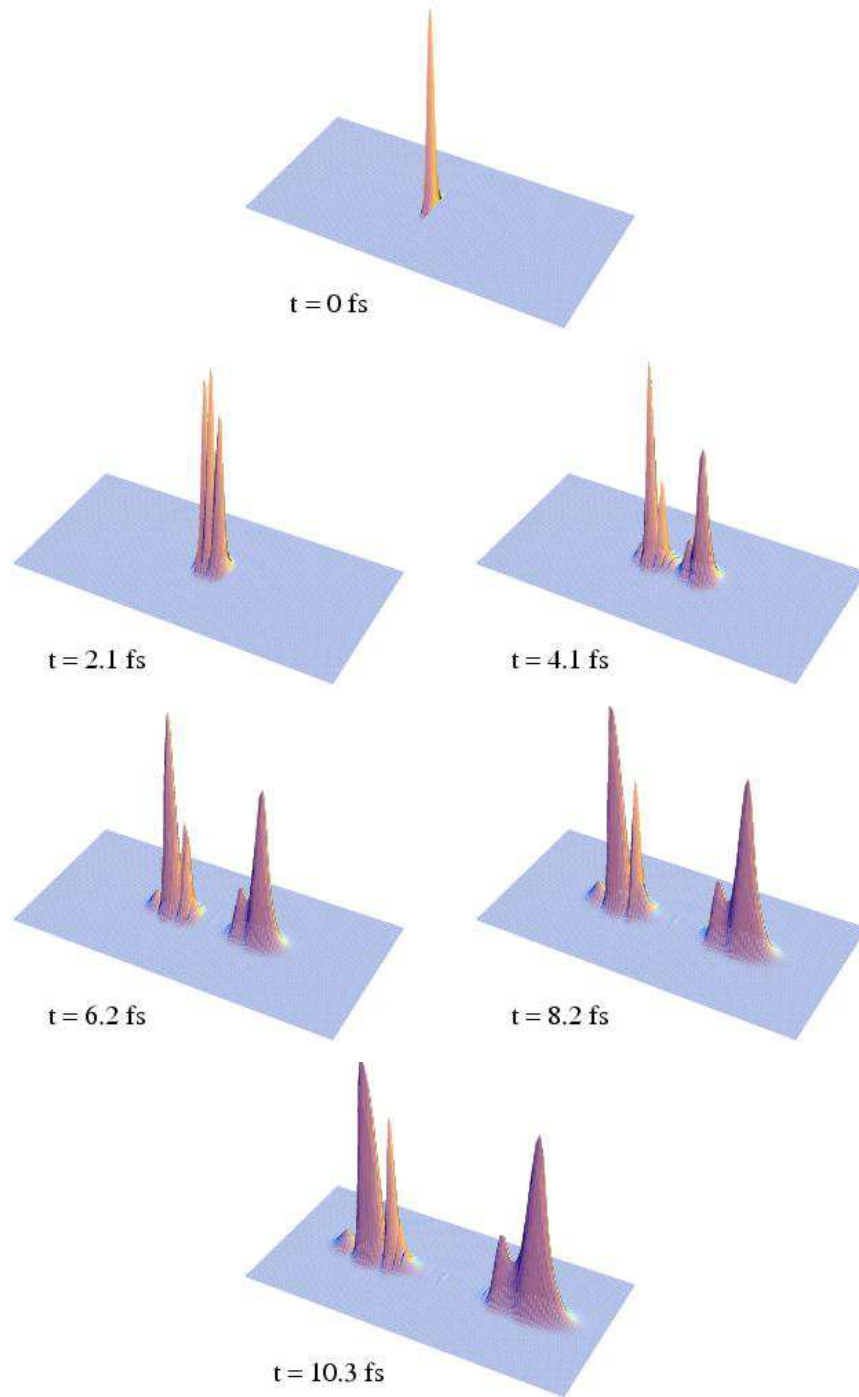


FIG. 6: Snapshots of the broad-energy wave packet scattering from the double barrier potential with  $\alpha = 90^\circ$ .

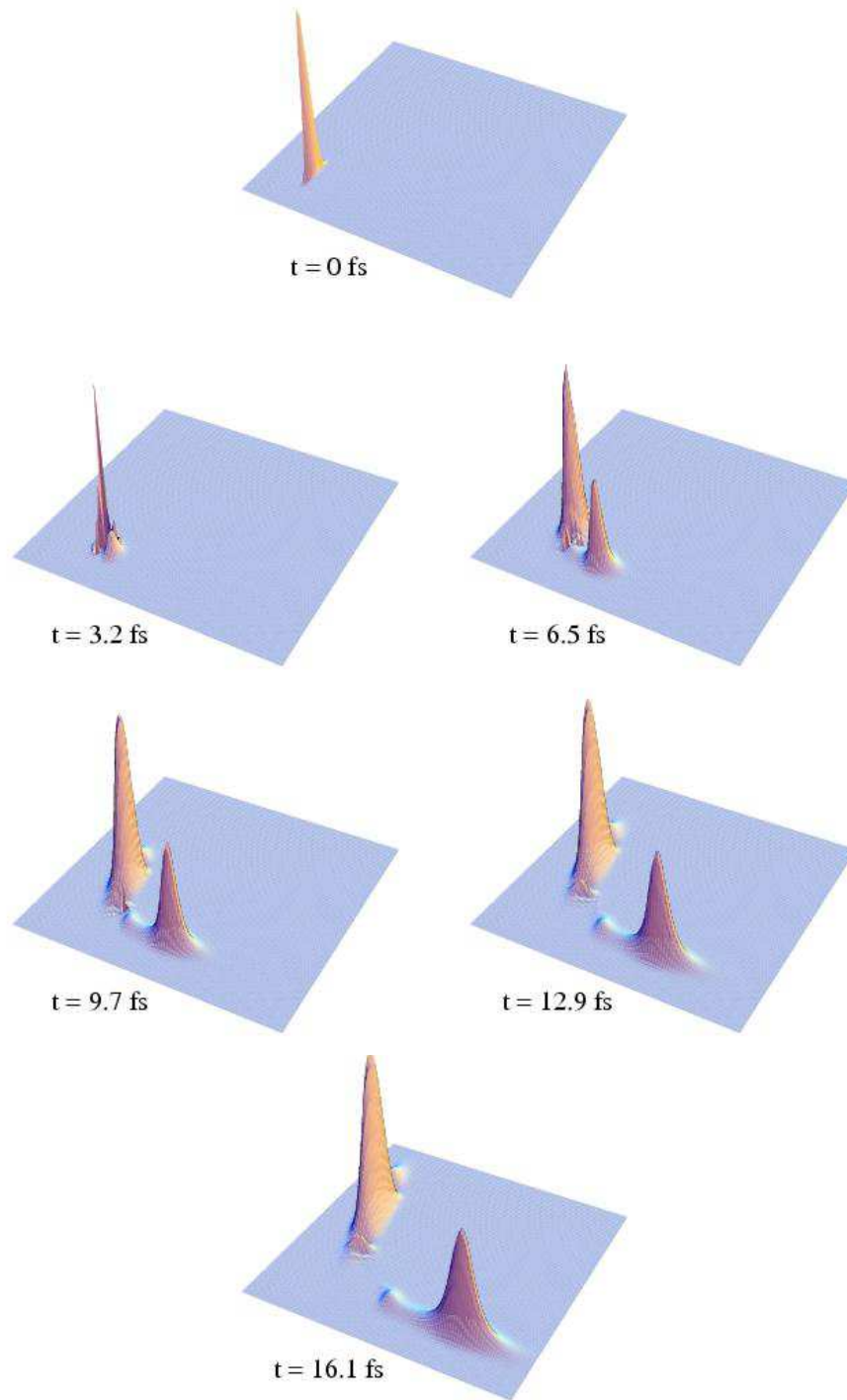


FIG. 7: Snapshots of the broad-energy wave packet scattering from the double barrier potential with  $\alpha = 52^\circ$ .

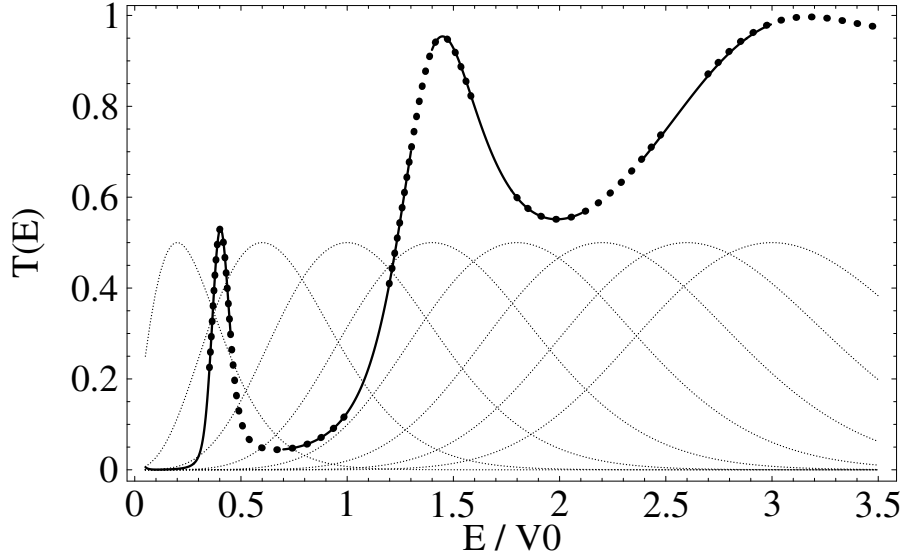


FIG. 8: Continuous transmission spectrum for the double barrier potential with  $\alpha = 52^\circ$ . Eight broad-energy wave packets with mean energies  $\bar{\mathcal{E}}/V_0 = 0.2, 0.6, 1.0, 1.4, 1.8, 2.2, 2.6$ , and  $3.0$  have been used to obtain the corresponding segments of the final curve. The agreement between these overlapping segments demonstrates that the transmission curve is independent of the choice of  $\bar{\mathcal{E}}$ .

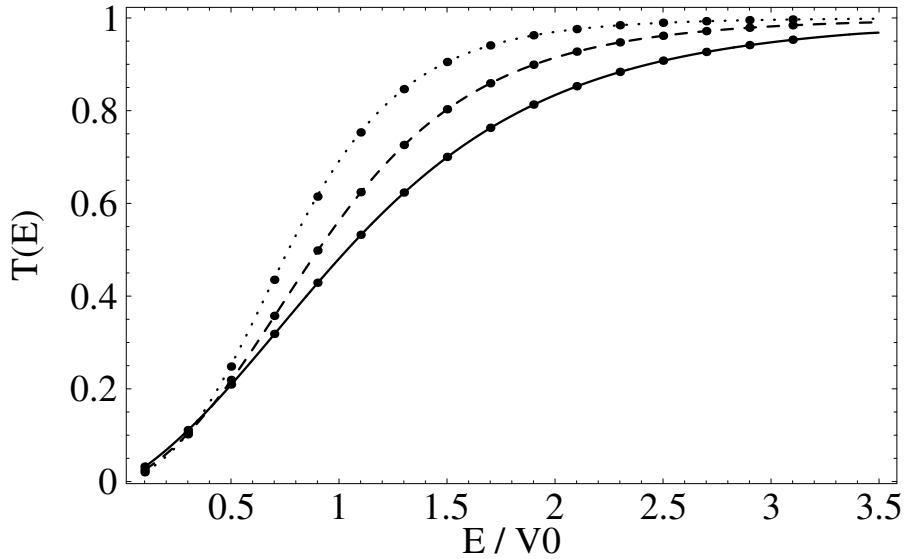


FIG. 9: Continuous transmission spectra for the single barrier potential with orientation angles  $\alpha = 52^\circ$  (solid),  $62^\circ$  (dashed) and  $90^\circ$  (dotted). Points on each curve represent the corresponding transmission coefficients calculated using the direct method.

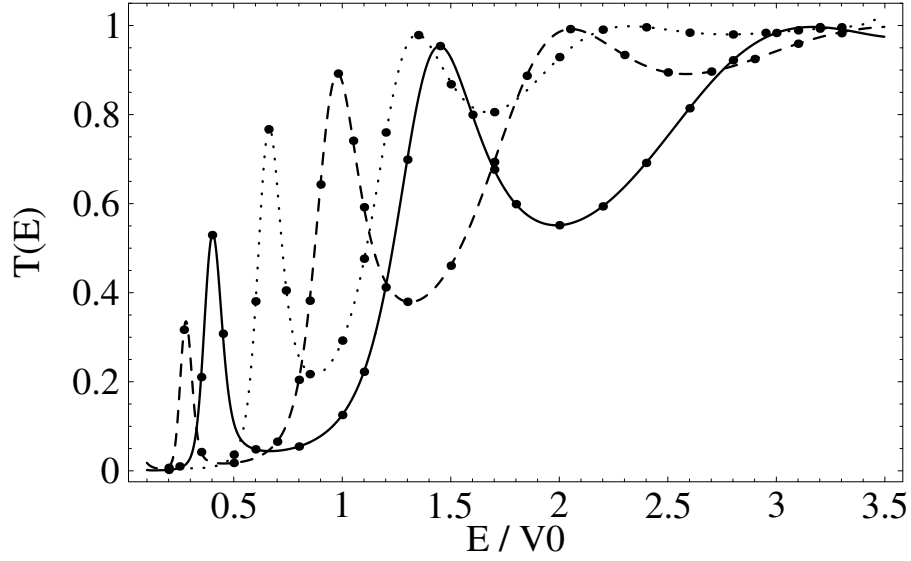


FIG. 10: Continuous transmission spectra for the double barrier potential with orientation angles  $\alpha = 52^\circ$  (solid),  $62^\circ$  (dashed) and  $90^\circ$  (dotted). Points on each curve represent the corresponding transmission coefficients calculated using the direct method.

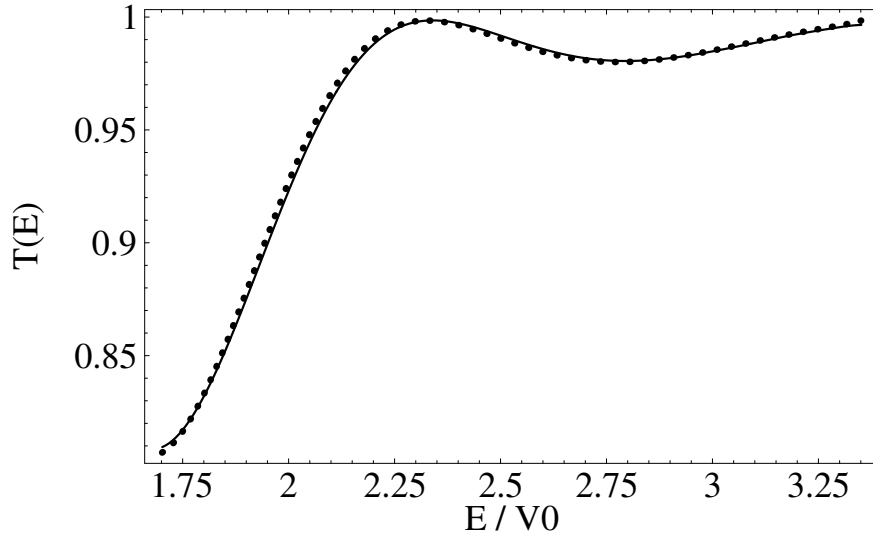


FIG. 11: Transmission curves for the double barrier potential with  $\alpha = 52^\circ$ , obtained using the accuracy factor  $\beta = 1.0$  (solid) and  $\beta = 1.2$  (dotted). The agreement between the two curves demonstrates that good convergence has already been achieved at  $\beta = 1.0$ .

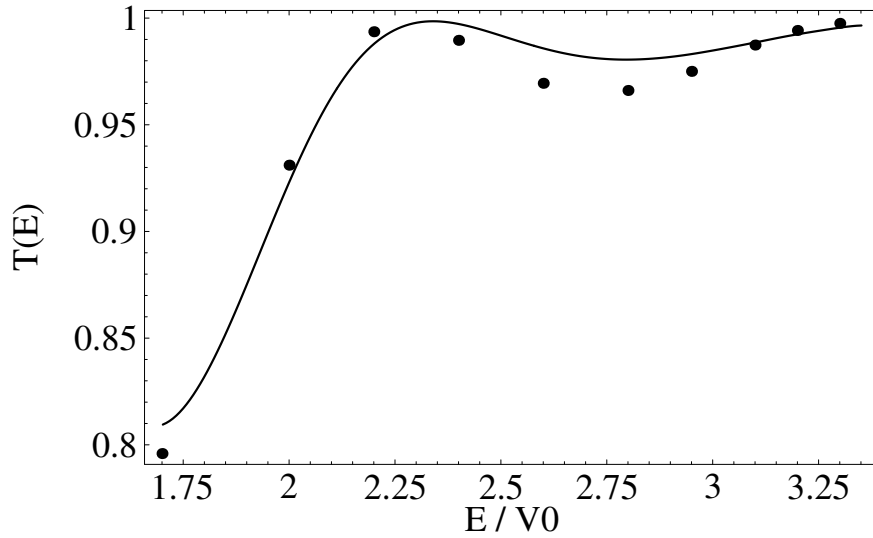


FIG. 12: Transmission curve for the double barrier potential with  $\alpha = 52^\circ$  vs. direct method transmission points. Both results have been obtained using the accuracy factor  $\beta = 1.0$ . Differences between the transmission curve and its corresponding transmission points suggest that the direct method does not achieve complete convergence at  $\beta = 1.0$ .

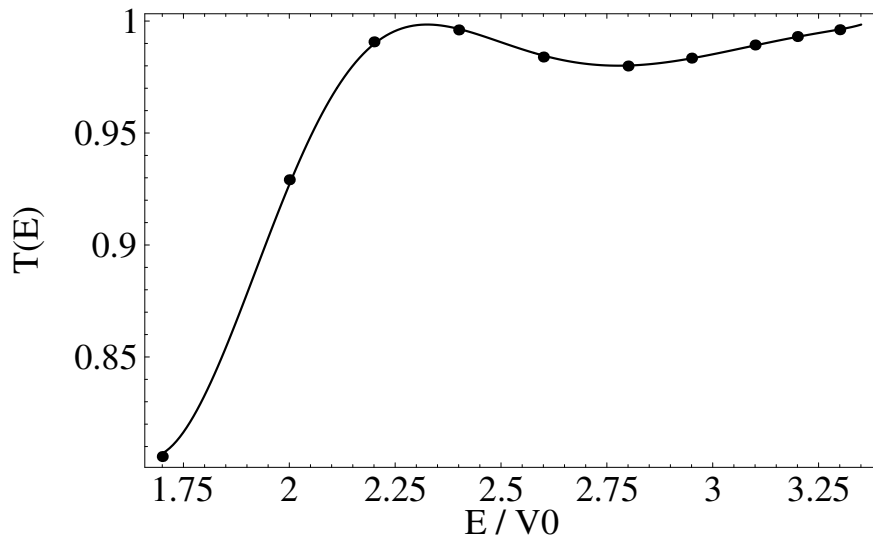


FIG. 13: Transmission curve for the double barrier potential with  $\alpha = 52^\circ$  vs. direct method transmission points. By increasing the accuracy factor  $\beta$  of the direct method from 1.0 to 2.0, we arrive at an agreement between the transmission curve and its corresponding transmission points. This suggests that the direct method requires  $\beta > 1.0$  for complete convergence.